Accepted refereed manuscript of:

Manuscript Details

Manuscript number	ICARUS_2016_477
Title	Abiotic versus biotic iron mineral transformation studied by a miniaturized backscattering Mössbauer spectrometer (MIMOS II), X-ray diffraction and Raman spectroscopy
Article type	Research paper

Abstract

Searching for biomarkers or signatures of microbial transformations of minerals is a critical aspect for determining how life evolved on Earth, and whether or not life may have existed in other planets, including Mars. In order to solve such questions, several missions to Mars have sought to determine the geochemistry and mineralogy on the Martian surface. This research includes the two miniaturized Mössbauer spectrometers (MIMOS II) on board the Mars Exploration Rovers Spirit and Opportunity, which have detected a variety of iron minerals on Mars, including magnetite ($Fe^{2+}Fe^{3+}_2O_4$) and goethite (α-FeO(OH)). On Earth, both minerals can derive from microbiological activity (e.g. through dissimilatory iron reduction of ferrihydrite by Fe(III)-reducing bacteria). Here we used a lab based MIMOS II to characterize the mineral products of biogenic transformations of ferrihydrite to magnetite by the Fe(III)-reducing bacteria Geobacter sulfurreducens. In combination with Raman spectroscopy and X-ray diffraction (XRD), we observed the formation of magnetite, goethite and siderite. We compared the material produced by biogenic transformations to abiotic samples in order to distinguish abiotic and biotic iron minerals by techniques that are or will be available onboard Martian based laboratories. The results showed the possibility to distinguish the abiotic and biotic origin of the minerals. Mossbauer was able to distinguish the biotic/abiotic magnetite with the interpretation of the geological context (Fe content mineral assemblages and accompanying minerals) and the estimation of the particle size in a non-destructive way. The Raman was able to confirm the biotic/abiotic principal peaks of the magnetite, as well as the organic principal vibration bands attributed to the bacteria. Finally, the XRD confirmed the particle size and mineralogy

Keywords	Bio-magnetite; Mössbauer spectroscopy; Raman spectroscopy; iron oxides; XRD
Corresponding Author	Emmanuel Lalla
Corresponding Author's Institution	Extreme Light Infrastructure (ELI) – Nuclear Physics, IFIN–HH
Order of Authors	Cristina Markovski, James M. Byrne, Emmanuel Lalla, A. Diego Lozano-Gorrin, Goestar Klingelhoefer, Fernando Rull, Andreas Kappler, Thorsten Hoffmann, Christian Schröder
Suggested reviewers	Fernando Gazquez, Pablon Sobron, Jung-Fu Lin, Jose J. Velazquez Garcia, Alejandro Rodriguez-Navarro

Submission Files Included in this PDF

File Name [File Type]

Letter to the Editor_Final.docx [Response to Reviewers]

Highlight.docx [Highlights]

Manuscript_Final.docx [Manuscript File]

List of Figures_Final.docx [Figure]

Figure-1.tif [Figure]

Figure-2.tif [Figure]

Figure-4.tif [Figure]

List of Tables_Final.docx [Table]

Submission Files Not Included in this PDF

File Name [File Type]

Figure-3.PNG [Figure]

To view all the submission files, including those not included in the PDF, click on the manuscript title on your EVISE Homepage, then click 'Download zip file'.

Dear Ms Scalzo,

We thank you for your efforts in helping during the review process of this manuscript. We have carefully considered all the points which have been raised by the reviewer and feel that they have contributed to improving the quality of the manuscript. The details of our changes are included herewith:

Reviewer (Minor corrections)
➔ *We appreciate the time and effort the reviewer has taken to evaluate the manuscript and are pleased with their opinion.*

We have considered the modifications that you recommended along the paper such as experimental campaigning to experiments, minor corrections on the references, small vocabulary corrections, etc.

Line 38: With the interpretation of the geological context and
We have added the geological context: (Fe content mineral assemblages and accompanying minerals).

Line 158: in situ measurements were carried out which correspond to samples where Mössbauer data was collected throughout the course of the experiment.
We rephrased the sentence is simple way: *in situ* Mössbauer measurements were carried out throughout the course of the experiment on each samples and it preparation.

Line 209: You could say here in which region of the spectrum
Based on the nature of Mössbauer spectroscopy, it is not common to refer to specific regions within a spectrum (e.g. as is the case for Raman), but instead discuss the presence of doublets or sextets. Therefore, we do not think defining the specific region of the spectrum will improve the interpretation of the data.

Line 212: You could say here in which region of the spectrum
See comment above

Line 296: Can you competently rule out the presence of remainders from the growth medium?
We removed this part by mentioning the existence of the organic substances due to the biochemical process.

Line 311: MIMOS II instrument, with the in situ experiments only looking at the very bottom layer of the iron layer which was undergoing microbial transformation. Is it possible that some conversion happens during the filtering stage?
The filtering removed the liquid fraction of the media which contains dissolved salts and the electron donor within a time frame of under 5 minutes. Consequently, there are no microbial transformation processes which could take place during or after filtration of the samples. As samples were measured directly after filtration under anoxic conditions, we do not consider that further crystallization took place in the samples.

Line 359: FH-AQDS-13 is calculated to be higher than those previously reported. Is there an implication for this?
We clarified by adding on the sentence: "..and showing a higher concentration of ferrous magnetite."

Figure 3. It has been corrected and improved.

Table 1. What is the difference between these two rows of "magnetite nanophases"? You may explain it in the table caption.
We have updated the figure caption to include:
"[a]Superparamagnetic magnetite - magnetic ordering prevented by small particle size.
[b]Magnetically ordered magnetite that has not reached full hyperfine splitting because of small particle size and/or impurities
[c]Values from Morris et al. (2008), averaging all magnetite and goethite measurements obtained in Gusev Crater with Mars Exploration Rover Spirit. Uncertainties quoted are standard deviations (2σ)."
"

HIGHLIGHTS:

Analysis of the mineral products of biogenic transformations of ferrihydrite to magnetite by the Fe(III)-reducing bacteria *Geobacter sulfurreducens* using the lab based MIMOS II from NASA-MER Mission.

A complete XRD and Raman mineralogical characterization has been carried on the different bio-mineralization processes for complementing the research.

The use of Mössbauer spectroscopy in combination with XRD and Raman spectroscopy presents an interesting combined system for the search of life, especially those focused on Martian mission.

1 **Abiotic versus biotic iron mineral transformation studied by a miniaturized**

2 **backscattering Mössbauer spectrometer (MIMOS II), X-ray diffraction and Raman**

3 **spectroscopy**

4 C. Markovski[1], J. M. Byrne[2], E. Lalla[3,4*], A. D. Lozano-Gorrín[5], G. Klingelhöfer[1], F. Rull[6],

5 A. Kappler[2], T. Hoffmann[1] and C. Schröder[7]

6 [1]Institut für Anorganische Chemie und Analytische Chemie, Johannes Gutenberg Universität

7 Mainz, Staudinger Weg 9, 55128 Mainz, Germany.

8 [2]Geomicrobiology, Center for Applied Geoscience, Eberhard Karls Universität Tübingen,

9 Sigwartstrasse 10, 72076 Tübingen, Germany.

10 [3]Centre for research in earth and space science, York University, Petrie Science Building,

11 4700 Keele St, Toronto, M3J 1P3, Ontario, Canada.

12 [4]Austrian Space Forum, Sillufer 3a, Innsbruck, 6020, Austria

13 [5]Departamento de Física, Universidad de La Laguna, 38200 San Cristóbal de La Laguna,

14 Santa Cruz de Tenerife, Spain.

15 [6]Unidad Asociada UVa-CSIC a traves del Centro de Astrobiologia Edificio INDITI, Parque

16 Tecnologico de Boecillo, Parcela 203, E-47151 Boecillo (Valladolid), Spain.

17 [7]Biological and Environmental Sciences, Faculty of Natural Sciences, University of Stirling,

18 Stirling FK9 4LA, Scotland, UK.

19

20 *Corresponding author: elalla@yorku.ca

21   **Abstract**

22   Searching for biomarkers or signatures of microbial transformations of minerals is a critical

23   aspect for determining how life evolved on Earth, and whether or not life may have existed

24   in other planets, including Mars. In order to solve such questions, several missions to Mars

25   have sought to determine the geochemistry and mineralogy on the Martian surface. This

26   research includes the two miniaturized Mössbauer spectrometers (MIMOS II) on board the

27   Mars Exploration Rovers Spirit and Opportunity, which have detected a variety of iron

28   minerals on Mars, including magnetite ($Fe^{2+}Fe^{3+}_2O_4$) and goethite (α-FeO(OH)). On Earth,

29   both minerals can derive from microbiological activity (e.g. through dissimilatory iron

30   reduction of ferrihydrite by Fe(III)-reducing bacteria). Here we used a lab based MIMOS II

31   to characterize the mineral products of biogenic transformations of ferrihydrite to magnetite

32   by the Fe(III)-reducing bacteria *Geobacter sulfurreducens*. In combination with Raman

33   spectroscopy and X-ray diffraction (XRD), we observed the formation of magnetite, goethite

34   and siderite. We compared the material produced by biogenic transformations to abiotic

35   samples in order to distinguish abiotic and biotic iron minerals by techniques that are or will

36   be available onboard Martian based laboratories. The results showed the possibility to

37   distinguish the abiotic and biotic origin of the minerals. Mossbauer was able to distinguish

38   the biotic/abiotic magnetite with the interpretation of the geological context (Fe content

39   mineral assemblages and accompanying minerals) and the estimation of the particle size in a

40   non-destructive way. The Raman was able to confirm the biotic/abiotic principal peaks of the

41   magnetite, as well as the organic principal vibration bands attributed to the bacteria. Finally,

42   the XRD confirmed the particle size and mineralogy

43   **Keywords**: Bio-magnetite, Mössbauer spectroscopy, Raman spectroscopy, iron oxides.

Introduction

44

45 The iron redox cycle is a significant process that takes place in most environments on Earth,

46 which can be conducted by both abiotic and microbial processes. In anoxic, pH-neutral

47 environments, microbial Fe(II)-oxidation is driven by either nitrate reducing bacteria (e.g.

48 *Acidovorax* sp. BoFeN1), photoferrotrophic bacteria (e.g. *Rhodopseudomonas palustris*

49 strain TIE-1) or neutrophilic microaerophilic bacteria (e.g. *Gallionella leptothrix*) (Kappler

50 et al., 2005; Kappler and Newman, 2004; Kappler and Straub, 2005). The other half of the

51 Fe cycle is driven by microbial Fe(III) reduction, either intracellularly by magnetotactic

52 bacteria (Blakemore, 1975) or outside of the cell wall by dissimilatory iron reducing bacteria

53 (DIRB) such as *Shewanella oneidensis* and *Geobacter sulfurreducens* (Lovley and Phillips,

54 1988, 1986). DIRB combine the oxidation of an organic substrate (e.g. acetate or lactate) or

55 hydrogen with the reduction of poorly crystalline, short range ordered, Fe(III) minerals (e.g.

56 ferrihydrite $(Fe^{3+})_2O_3 \bullet 0.5H_2O$) and can lead to the formation of many different iron mineral

57 phases and compounds including goethite, magnetite, green rust and siderite ($FeCO_3$) (Byrne

58 et al., 2011). The mineralogical composition of these products of reduction depends on

59 geochemical parameters, including Fe(III) reduction rate, pH, temperature and the presence

60 of electron shuttles (e.g. riboflavin, quinones and humic acids) (O'Loughlin et al., 2010;

61 Piepenbrock et al., 2011). Furthermore, a recent study suggests that magnetite can act as both

62 an electron donor and an electron acceptor to different types of Fe metabolizers depending

63 on the redox conditions (Byrne et al., 2015). In this regard, understanding the mineralogical

64 products of biomineralization processes can help to detect signatures of microbial

65 interactions with fluid, rocks, mineral deposits and subsequent diagenesis.

66   Several terrestrial environments where microbially driven Fe(III) reduction processes

67   occur (Léveillé, 2009; Rothschild and Mancinelli, 2001) have been identified, such as Rio

68   Tinto (SW Spain), Western Australian salt lake sediments (SW, Australia) and Ten Graben

69   fault system of Green River (Utah, USA), have been proposed as terrestrial analogues to the

70   types of conditions on Mars where iron cycling could have taken place (Nixon et al., 2012;

71   Ruecker et al., 2016). These terrestrial analog systems allude to the existence of Fe(III)-

72   oxyhydroxide bio-signatures and fossilized microorganisms, with Fe(III)-oxyhydroxides

73   susceptible to recrystallization to more stable forms (Léveillé, 2009; Nixon et al., 2012;

74   Parenteau et al., 2014; Ruecker et al., 2016). Utilizing Laboratory studies and natural

75   analogues can be used to help identify bio-signatures preserved from the past (NASA´s Mars

76   Exploration Rover Mission *Spirit*), current (NASA´s Mars Exploration Rover Mission

77   *Opportunity*; Mars Science Laboratory (MSL) *Curiosity*) or future Mars missions (ESA-

78   ExoMars rover; NASA Mars 2020) (Bish et al., 2013; Bost et al., 2015).

79   One of the most important techniques for characterizing Fe minerals on Mars is ^{57}Fe

80   Mössbauer spectroscopy. This technique is capable of determining the oxidation state of iron,

81   as well the mineralogy and the magnetic structure of different Fe mineral phases (Helgason,

82   2004). Indeed, two miniaturized Mössbauer spectrometers (MIMOS II) were part of the suite

83   of analytical instruments carried on board the two Mars rovers Spirit and Opportunity, which

84   landed on January 4, 2004 and January 25, 2004, respectively (Klingelhöfer et al. 2003). The

85   data collected by these vehicles have provided a significant insight into the mineralogy of

86   iron compounds on the Martian surface (Klingelhöfer et al., 2004, 2003, Morris et al., 2010,

87   2006, 2004). Raman and X-ray diffraction (XRD) techniques are among the payload of other

88   current and future space missions (Bish et al., 2013; Bost et al., 2015, 2013). This includes

89 the CheMin XRD system on the NASA MSL Curiosity mission (Bish et al., 2013) and Raman

90 instruments such as the SHERLOC (Scanning Habitable Environment with Luminiscence for

91 Organics and Chemical Instrument) system, the Raman SuperCam that were selected for the

92 NASA Mars 2020 rover, and the Raman Laser Spectrometer (RLS) of the ESA ExoMars

93 rover (Grossman, 2013; Hutchinson et al., 2014; Léveillé, 2009; Wang et al., 2015).

94   In this study, we investigated the formation of biogenic magnetite nanoparticles

95 through microbial Fe(III)-reduction by the DIRB *Geobacter sulfurreducens* in the presence

96 and absence of the electron shuttling compound Anthraquinone-2,6-disulfonate (AQDS).

97 The presence of the electron shuttle is expected to greatly increase the speed of microbial

98 Fe(III)-reduction compared to experiments in which it is not present. The presence/absence

99 of AQDS should therefore have an impact on the type of mineral phases which are produced

100 during the reduction and affect their stoichiometry (i.e. Fe(II)/Fe(III) ratio). The

101 spectroscopic and mineralogical characteristics of these minerals were compared to those of

102 minerals formed from abiotic syntheses in laboratory and to natural samples. The main goal

103 of this study is to distinguish between iron minerals formed through abiotic and biotic process

104 by techniques that are or will be available onboard Martian based laboratories. In most cases,

105 Mössbauer spectroscopy can only be applied to dry powdered materials or embedded in a

106 solid matrix such as in ice or on a filter. Here, however, we use the MIMOS II instrument to

107 analyze in situ, a solid material that has deposited from an aqueous suspension. Our study is

108 analogous to experiments conducted by Zegeye et al. (2010) who performed *in situ*

109 monitoring of lepidocrocite bioreduction and magnetite formation by backscattering

110 Mössbauer spectroscopy (Zegeye et al., 2011, 2010).

111

Experimental setup

Preparation of ^{57}Fe enriched Fe(III)- oxyhydroxide

A starting precipitate of ^{57}Fe enriched (~12%) Fe(III)-(oxyhydr)oxide was prepared to enhance the signal-to-noise ratio of the Mössbauer spectrum obtained for sediment in water. Powdered naturally abundant isotope ^{NA}Fe(0) and pure ^{57}Fe(0) were separately dissolved in 0.7 M anoxic HCl in an anoxic glovebox (MBRAUN, 100% N_2 atmosphere) and continuously stirred overnight at 400 rpm leading to the formation of ^{NA}Fe^{2+} and ^{57}Fe^{2+}, respectively. The two solutions were filtered (0.22 μm syringe tip filter) to remove any solid precipitates, then mixed in a volume ratio of 10% ^{57}Fe and 90% ^{NA}Fe and removed from the glovebox. The ^{57}Fe (i.e. containing ~12% ^{57}Fe) enriched solution was oxidized using 400 μl H_2O_2 (37%) and stirred at 400 rpm for 2 hours to form an aqueous solution of acidified Fe^{3+}. KOH (5 M) was added dropwise to the Fe^{3+} solution, leading to the precipitation of the Fe(III)-oxyhydroxide, at a final pH=7. The precipitate was washed of additional ions by centrifugation (4000 rpm, 20 min) three times, with the supernatant discarded and the precipitate re-suspended in ultrapure H_2O. After the final centrifugation step, the material was kept in liquid suspension and put into a 20 ml headspace vial. The suspension was made anoxic (but not dried) by applying vacuum (5 min) followed by flushing with N_2 gas (30 seconds), with both steps repeated three times. The final concentration of iron in the Fe(III)-oxyhydroxide suspension was determined using the ferrozine assay (Stookey, 1970) to be 421 mmol l^{-1}.

Fe(III)-reduction experiments

133   Two separate experiments were carried out using the ferrihydrite at different times, with one

134   in 2013 and the second in 2014. For both sets of experiments, *Geobacter sulfurreducens*

135   bacteria were grown until the late log phase in basal medium (Ehrenreich and Widdel, 1994),

136   containing 25 mM acetate (electron donor), 40 mM fumarate (electron acceptor) and buffered

137   with 22 mM NaHCO$_3$. The bacteria were then centrifuged three times (4000 rpm; 20 min) to

138   remove the growth medium and washed with 30 mM NaHCO$_3$ in between centrifugation

139   steps. The final cell suspension was made up to a volume of 2 ml and the optical density at λ

140   = 600 nm (OD$_{600}$) measured at 0.385 abs and 0.372 abs (FlashScan 550, Analytik Jena,

141   Germany) for experiments in 2013 and 2014 respectively.

142   All Fe(III) reduction experiments were prepared in Plexiglas holders with a 500 µm bottom

143   thickness. For 2013 experiments, cultures were prepared up to a volume of 15 ml in the

144   glovebox using sterile, anoxic solutions and consisted of 50 mmol L^{-1} Fe(III)-

145   (oxyhydr)oxide, 20 mM acetate and 30 mM NaHCO$_3$. One of the cultures additionally

146   contained AQDS (10 µM) as an electron shuttle. Both culture experiments were sealed with

147   a rubber butyl stopper to maintain an anoxic environment. The culture experiments were

148   inoculated with 0.312 ml of *G. sulfurreducens* cell suspension immediately prior to loading

149   on to the MIMOS II device. The cultures are subsequently referred to as FH+AQDS-13 and

150   FH-AQDS-13.

151   For the 2014 experiment, the culture were prepared in a similar way, however it contained

152   double the concentration of iron material, i.e. 100 mmol L^{-1} Fe(III)-oxyhydroxide, 40 mM

153   acetate and 30 mM NaHCO$_3$. There was no AQDS present. The 2014 experiment was

154   inoculated with 0.644 ml of the *G. sulfurreducens* cell suspension, so approximately twice

155   as many cells as for the 2013 experiment. This culture is referred hereafter as FH-AQDS-14.

Analytical methods

156

157   During the 2014 experiments, *in situ* Mössbauer measurements were carried out throughout

158   the course of the experiment on each samples and it preparation. These *in situ* Mössbauer

159   spectra were collected by placing the culture incubation vessels onto a MIMOS II in

160   backscattering geometry at the Mössbauer Group of Mainz University (Germany) and left

161   for the duration of the experiment. The culture vessels during the 2013 experiments were

162   left on the MIMOS II, however the recorded spectra were not of sufficient quality due to their

163   lower iron concentrations. Following the reduction phase of each experiment, the contents of

164   each of the reaction vessels were filtered with Millipore swinnex filter holders and Millipore

165   membrane filters (0.45 µm - HAWP04700). The entire solution of these experiments were

166   passed through the filter and then dried under an N_2 atmosphere. Filtered samples were sealed

167   in between two layers of Kapton tape to inhibit oxidation of the samples during measurement,

168   and Mössbauer spectra were collected with the MIMOS II instrument. Spectra were

169   calibrated against alpha-iron at room temperature and fitted with an in house routine (Mbfit)

170   using Lorentzian and Voigt line profiles. Mbfit is based on the least-squares minimization

171   routine MINUIT (James, 2004). All Mössbauer fitting parameters are shown in Table 1 (i.e.

172   center shift (CS), quadrupole splitting (ΔE_Q), hyperfine field (B_{hf})).

173   Dried samples from the 2013 experiments (i.e. FH-AQDS-13 and FH+AQDS-13) were

174   analyzed using X-ray diffraction (XRD), with data collected using a Bruker D8 Discovery

175   Diffractometer equipped with a molybdenum $K_{\alpha 1}$ X-ray tube (λ= 0.71 Å) at the Institut für

176   Anorganische Chemie und Analytische Chemie of Mainz University (Germany). Total

177   scattering was measured between 5° and 40° 2θ. A comparison with a natural rock magnetite

178   standard has been done. The natural magnetite used belongs to the NASA Athena Reference

179   Samples (Aref 043) (Schröder, 2003). Magnetite sample was ground in an agate mortar and

180   fixed onto a polymer tape (Scotch). The data were refined using the Rietveld method

181   (Rietveld, 1969) and the FULLPROF software (Rodríguez-Carvajal, 1993). A pseudo-Voigt

182   function was used to describe the peak shape and a polynomial function with five refinement

183   coefficients for the background.

184   Spectroscopic Raman measurement were performed at the Unidad Asociada Uva-CSIC

185   (Valladolid, Spain) on the dried samples from the 2013 experiments (i.e. FH-AQDS-13 and

186   FH+AQDS-13). The Raman mineralogical characterization of the sample was performed by

187   micro-Raman spectroscopy, using a microscope Nikon Eclipse E600 coupled to a

188   spectrometer KOSI Holospec f/1.8i with a resolution of 5 cm^{-1} illuminated by a laser REO

189   LSRP-3501, He-Ne 632.8 nm. The detection was performed by a CCD Andor DV420A-OE-

190   130 with a resolution of 5 cm^{-1}. The laser power used is 14 mW with a spot diameter of 15

191   µm. The kapton cover of prepared samples produce strong Raman fluorescence. The material

192   was carefully extracted from the Plexiglas holders inside a chamber/bell with a nitrogen

193   atmosphere to avoid abiotic oxidation. Moreover, some natural iron-oxides, sulfate and

194   carbonate from the sample collection of the ESA-ExoMars Raman Laser Spectrometer (RLS)

195   database were measured and used as a reference materials. The reference samples stem (1)

196   from several fieldtrips to terrestrial analogues including Rio Tinto (Spain), Tenerife (Spain),

197   Svalbard (Norway), Faroe Island, etc. (Lalla et al., 2016, 2015; Sansano et al., 2015) or (2)

198   were synthetized in the laboratory (Sansano-Caramazana, 2015). The spectral Raman

199   collection of the mineral phases has been obtained using standard Raman systems and the

200   RLS simulator system, processed and analyzed using the protocols for the ExoMars mission

201   (Hermosilla et al., 2012).

202   **Results**

203 *Mössbauer analysis*

204 Data were obtained for the FH-AQDS-14 experiment which was incubated at room

205 temperature on a MIMOS II throughout the microbial Fe(III) reduction over the course of 19

206 days (Figure 1a and b) and are consequently referred to as *in situ* measurements. Figure 1a

207 shows the recorded spectrum obtained for FH-AQDS-14 after 6 h, with a clear doublet visible

208 despite the fact that the starting precipitate (ferrihydrite) is suspended in liquid media. Figure

209 1b shows the recorded spectrum for FH-AQDS-14 after 19 days of incubation on the MIMOS

210 II, with the data clearly indicating the presence of both a doublet and sextet. After 19 days

211 the microbial Fe(III) reduction in the *in situ* experiments was stopped and the precipitates

212 were filtered. The filtered samples were then placed onto the MIMOS II again for further

213 analysis, with Figure 1c showing the spectrum from the FH-AQDS-14 filtered sample at

214 room temperature. It is clear from the figure that after 6 h, the sample displays a spectrum

215 corresponding to ferrihydrite, whilst after 19 days, the sample shows a clear sextet which

216 likely corresponds to magnetite. After filtration (Figure 1c), the sample displays a more

217 characteristic spectrum of magnetite, though additional peaks corresponding to ferrihydrite

218 and goethite appear to be present.

219 Figure 2 shows the data collected for FH-AQDS-13 (Figure 2a) and FH+AQDS-13 (Figure

220 2b) experiments measured at room temperature after filtration and loaded directly onto the

221 MIMOS II instrument. The Mössbauer spectra for a reference sample of magnetite (Athena

222 Reference Sample 043) is shown in Figure 2c for comparison and clearly shows the

223 tetrahedral and octahedral lattice sites expected for the mineral. Figure 2 indicates that

224 ferrihydrite FH-AQDS-13 was transformed mainly into pure magnetite, whilst

225 FH+AQDS-13 was transformed to magnetite, but with traces of siderite.

226 ***XRD***

227 XRD data shown in Figure 3 confirms that the only mineral phase present in sample FH-

228 AQDS-13 at the end of the experiment was magnetite whereas sample FH+AQDS-13

229 contained both magnetite and siderite, confirming the Mössbauer results. The structure of

230 magnetite is centrosymmetric and shows cubic symmetry with space group *Fd-3m*. The

231 lattice parameter for FH-AQDS-13 and the FH+AQDS-13 samples show values around 8.30

232 Å which is comparable to known standards. The average crystallite sizes for both samples

233 (also known as the coherent scattering domain) has been determined through the use of the

234 Scherrer equation (Scherrer, 1918), being around 27-30 nm.

235 ***Raman analysis***

236 Raman spectroscopy was carried out on selected areas of samples FH+AQDS-13 and FH-

237 AQDS-13 (Figure 4) and compared to reference bands for several different iron minerals

238 (Table 2) (Hanesch, 2009). The measured data has been processed by a Gaussian curve fitting

239 analysis on each band to obtain the correct band position of the different minerals phases on

240 the spectra. The fitting has been obtained by using the commercial program Bruker OPUS

241 and following the standard procedure: spectra smoothing (if it is needed), background

242 subtraction, normalization and interactive curve fitting (by Levenberg-Marquardt and/or

243 Local Least Squares methods).

244 The results show the existence of several mineral oxides such as hematite, magnetite, siderite,

245 and possibly poorly crystalline goethite in the band fitting (Figure 4 and Table 3). The bands

246 in the region at 120 to 220 cm^{-1} belong unambiguously to the siderite being present on the

247 different spectra. Secondly, the bands of the region 220-420 cm^{-1} have been assigned to the

248   vibration of hematite (~225, ~245, ~290 cm^{-1}), siderite (~287 cm^{-1}), goethite (~244, ~300

249   and ~385 cm^{-1}) and magnetite (310 cm^{-1}). However, the bands corresponding to

250   FH-AQDS-13 (Figure 4a and 4b) are more intense compared to FH+AQDS-13 (Figure 4c

251   and 4d) due to the influence of goethite presenting the strongest vibration in this band region

252   (according to the band fitting). On the other hand, the region 420-550 cm^{-1} presents the

253   vibration of goethite (~480 cm^{-1}), magnetite (~530 cm^{-1}), hematite (~500 cm^{-1}) and siderite

254   (~500 cm^{-1}). The bands on FH-AQDS-13 obtained by the curve fitting show a strong

255   influence caused by amorphous goethite (Figure 4a and 4b).

256   The region from 560 to 800 cm^{-1} can be assigned mainly to the magnetite (~650 cm^{-1}),

257   possibly goethite (681 cm^{-1}), hematite (~610 and ~660 cm^{-1}) and siderite (~720 cm^{-1}). Finally,

258   the region within the 1200-1650 cm^{-1} presents a mixture of bands that belong to

259   hematite/goethite magnon (~1350 cm^{-1}) and organics (~1314, ~1422, ~1545 and ~1575 cm^{-1}).

260

261   The magnetite bands are clearly visible at 300, 532 and 661 cm^{-1} which are in close agreement

262   with other studies (Hanesch, 2009; Shebanova and Lazor, 2003). The intense bands

263   corresponding to the A_{1g} mode at 667 cm^{-1} presents a variation of magnetite measured in other

264   studies. The A_{1g} oxide peak of magnetite is shifted toward higher wave numbers in the bio-

265   magnetite (700 cm^{-1}) compared to that of the inorganically produced magnetite (670 cm^{-1})

266   (Jimenez-Lopez et al., 2010). In previous studies, it has been found that a transition to an

267   orthorhombic phase on a starting oxidation process produces a displacement of the A_{1g} to

268   higher values (Shebanova and Lazor, 2003). The second magnetite band between 532 and

269   550 cm^{-1} is reported as the mode F_{2g} and is observed to be sensitive to possible defects in the

270   crystal structure as well as the presence of vacancies and interstitial cations. Furthermore,

271   other studies suggest that the F_{2g} band below to 500 cm^{-1} can be attributed to the occurrence

272   of hematite (de Faria et al., 1997; Hanesch, 2009; Shebanova and Lazor, 2003). The siderite

273   presents the strongest band at 182, 287, 731 and 1090 cm^{-1} (Hanesch, 2009; Rull et al., 2004).

274   The band fitting also reveals the existence of hematite and it presents as a combination of

275   several vibrations at 225, 245, 291, 410, 500 and 611 cm^{-1} with the magnon at 1321 cm^{-1}

276   (Hanesch, 2009). In the case of the possible goethite presence, the principal vibrations are at

277   244, 299, 385, 480 and 681 cm^{-1} being the most commonly used for the identification in

278   complex vibrational analysis (de Faria et al., 1997; Hanesch, 2009; Rull et al., 2004). The

279   bands at the aforementioned positions are very weak and broadened, due to poorly

280   crystallized goethite, which is combined with other oxide mineral phases (magnetite and

281   hematite).

282   When considering the Raman bands of biological component, the most intense vibrations

283   were detected between 1300 and 1600 cm^{-1}, which can be assigned to the active modes D

284   and G of the C-C bonds vibrations from carbonaceous materials. The band fitting

285   corresponding to this vibrational region presents several medium intensity vibrations at 1314,

286   1422 and 1565 cm^{-1} according to the best fitting analysis. The bands at 1314 and 1422 cm^{-1}

287   can be assigned to the D double modes D1 and D2, which is in agreement with other studies

288   (Ferrari, 2007). However, it has been found during band fitting that an influence of other

289   magnon vibrations of hematite/goethite phases on 1350 cm^{-1} (Hanesch, 2009; Rull et al.,

290   2007) is possible. The band G has also been observed (see Table 3), showing a distorted

291   structure clearly detectable by the broad bands. The vibrations at 2903 and 2961 cm^{-1}

292   correspond to the C-H vibrational regions, which could be assigned to symmetric and

293   asymmetric stretching of the –CH$_3$ from the organic matter (Böttger et al., 2012; Pereira et

294   al., 2007). Furthermore, the *G. sulfurreducens* Raman vibration bands can be assigned to the

295   peaks detected along the different spectra measurements. In this regard, several vibrations

296   have been identified considering the following regions: (1) the C-H stretching region bands

297   on 2900-3000 cm^{-1}; (2) the CH deformation vibrational region between 1300 and 1450 cm^{-1};

298   and (3) the C=O stretching vibration zone in 1650 to 1800 cm^{-1} approximately (el-Kabbani

299   et al., 1991; Kudelski, 2005).

Discussion

301   The *in situ* Mössbauer spectrum for FH-AQDS-14 after 6 h is dominated by the presence of

302   a doublet corresponding to ferrihydrite. After 19 days the sample is still dominated by a

303   central ferric doublet, although a sextet is clearly evident. In the filtered sample however

304   (Figure 1c), it is clear that the Mössbauer spectrum displays two sextets corresponding to (1)

305   tetrahedrally coordinated iron denoted Fe^{3+}_{tet}, and (2) octahedrally coordinated Fe which

306   includes both Fe^{2+} and Fe^{3+}, often denoted $Fe^{2.5+}_{oct}$ with an additional goethite phase. This

307   apparent difference in the sample before and after filtration is likely due to the nature of the

308   MIMOS II instrument, with the *in situ* experiments only looking at the very bottom layer of

309   the iron layer which was undergoing microbial transformation. A gradient in the reaction

310   likely existed with most reduction taking place in the top portion of the sample where the

311   mineral is more exposed to the solution (Dippon et al., 2015).When the sample was filtered,

312   it was mixed and so the top fraction and bottom fraction were mixed and thus yielded the

313   sextet as seen in Figure 1c. The goethite phase present in the filtered sample of FH-AQDS-14

314   was fitted with a sextet in which the hyperfine magnetic field (B_{hf}) value (Table 1) is smaller

315   than that of well-crystalline goethite, indicating that the goethite has very low crystallinity or

316   consists of very small particles.

317 In the experiments carried out in 2013, sample FH-AQDS-13 (Figure 2a) appears to have

318 more well-defined sextets than sample FH+AQDS-13 (Figure 2b). The broadened lines and

319 additional broad sextet in these spectra can be explained by a lower degree of crystallinity

320 possibly because of impurities in the magnetite structure, e.g. the incorporation of organic

321 matter, and/or small particle sizes. In magnetically ordered phases, which present as sextets

322 in Mössbauer spectra, these influences reduce the strength of the internal B_{hf}. A range of

323 degrees of crystallinity then results in broad lines skewed towards smaller B_{hf} values. Small

324 particle sizes, generally 30 nm or less, can additionally lead to an effect called

325 superparamagnetism (Daniels and Rosencwaig, 1969). The particle sizes are then in the range

326 of individual magnetic domains and random thermal movement of the particles leads to a net

327 zero magnetic field and magnetic ordering appears to collapse, which manifests itself as a

328 paramagnetic doublet in the Mössbauer spectrum instead of a magnetically ordered sextet

329 (Daniels and Rosencwaig, 1969; Dezsi et al., 2008). Superparamagnetism appears to be

330 visible in sample FH+AQDS-13 with the very broad lines in the Mössbauer spectrum (Figure

331 2b) in agreement with previous studies which have shown the samples prepared in the

332 presence of electron shuttles (e.g. AQDS) tend to be smaller in diameter than those without

333 (Byrne et al., 2011). Furthermore, the FH+AQDS-13 sample clearly contains siderite which

334 is likely due to the enhanced rate of microbially driven Fe(III) reduction, due to the presence

335 of AQDS, resulting in an excess of Fe^{2+} in solution which can further react with the CO_3^{2-}

336 present in solution from the buffer system and lead to the precipitation of siderite (Cornell

337 and Schwertmann, 2003; Hansel et al., 2003; Liu et al., 2009).

338 The parameters obtained from fitting the magnetite spectra closely correspond to the values

339 expected for magnetite (Table 1). All of the hyperfine parameters determined are in general

340   smaller than expected, however this is likely due to the sample exhibiting poorer magnetic

341   ordering at room temperature than well-crystalline, stoichiometric magnetite (Figure 2c).

342   Neglecting potential differences in *f*-factor for the different Fe lattice positions, the

343   stoichiometric ratio (x=Fe(II)/Fe(III)) of magnetite can be determined by comparing the

344   relative areas of the two sextets according to the following equation (Da Costa et al., 1995;

345   Daniels and Rosencwaig, 1969):

346
$$x = \frac{0.5\ Fe^{2.5+}_{oct}}{0.5\ Fe^{2.5+}_{oct} + Fe^{3+}_{tet}} \quad (1)$$

347   Using equation 1 it is seen that magnetite formed in FH+AQDS-13 (x = 0.25) is more

348   oxidized than perfectly stoichiometric magnetite (x = 0.5). The iron in magnetite formed in

349   FH-AQDS-13 (x = 0.65) is more reduced than stoichiometric magnetite. The difference is

350   thought to be due to the faster reduction rate in the presence of AQDS, leading to the

351   formation of superparamagnetic magnetite nanoparticles. However, this result also suggests

352   that the presence of electron shuttles might in fact lead to the formation of rather oxidized

353   magnetite. Since electron shuttles such as AQDS are organic compound, it might indicate

354   that magnetite found in regions with low stoichiometry can be linked to the presence of

355   organic substance. The relative ratio of Fe(II)/Fe(III) in the magnetite in FH-AQDS-13 is

356   calculated to be higher than those previously reported and showing a higher concentration

357   of ferrous magnetite (Veeramani et al., 2011). Moreover, the mineral phases measured are in

358   agreement with Veeramani *et al.*, (Veeramani et al., 2011), though here we have also

359   identified the presence of siderite.

360   The XRD results for our samples show smaller values for the lattice constant(8.30 Å) than

361   the 8.397 Å associated with stoichiometric magnetite (ICDD, n.d.; "Magnetite -

362   www.mindat.org," 2001). Maghemite has a smaller lattice constant of 8.33 Å, which is more

363   similar to our results, suggesting the samples to be partially oxidized which agrees with the

364   Mössbauer results for sample FH+AQDS (Wohlfarth and Arrott, 1982). It has also been seen

365   that the lattice parameters of pure and metal-substituted bio-magnetites tend to be smaller

366   compared to those of chem-magnetites where the bio-magnetite likely has a relatively more

367   compact crystal structure with fewer uncoordinated iron ions on the surface (Moon et al.,

368   2010). The average crystal size is around 27-30 nm for the FH+AQDS-13 and FH-AQDS-13,

369   being consistent with the Mössbauer observations of smaller B_{hf} values, broadened and

370   skewed lines, and superparamagnetism. Also, this result confirms the interpretation of other

371   studies (Byrne et al., 2011; Veeramani et al., 2011).

372   In the Raman results, the variation of A_{1g} mode corresponding to the magnetite could

373   becaused by the curve fitting or may be due to structural changes generated during the

374   microbial Fe(III) reduction where the oxidation process produces a displacement of the A_{1g}

375   to higher values. An estimation can be done by curve fitting relative band intensity of I_{685-90}/I_{650}

376   produced by the magnetite and the bio-magnetite, the results show the existence of two

377   Raman bands where the I_{685-90} is more intense (See Table 3b – Figure 3). Also, the

378   FH-AQDS-13 presents the possible existence of goethite due to the higher intensity of the

379   bands in the region between 220-420. Furthermore, it can be affirmed by the $I_{220-520}/I_{560-800}$,

380   which for FH-AQDS-13 is at approximately 0.5 and FH+AQDS-13 is 0.35 (Figure 3).

381   In the region from 2800 to 3100 cm^{-1}, the FH-AQDS-13 bands are more intense compared to

382   those of FH+AQDS-13 spectra and confirm that the *G. sulfurreducens* transformed the

383   starting material.

384   In general, the combination of Mössbauer, Raman and XRD technique allowed the detection

385   of several iron mineral phases and mineral structures. The magnetite was the main mineral

386   that formed as a result of microbial Fe(III) reduction by *G. sulfurreducens*. The Raman based

387   vibrational technique was able to detect hematite with the possibility of minor phases of

388   goethite, clearly distinguishable by the main vibrations and the curve-fitting. Mössbauer

389   spectra indicate oxidized magnetite in the FH+AQDS-13 samples. Oxidation of magnetite

390   leads to maghemite and eventually hematite formation, but these phases are difficult to

391   differentiate (Vandenberghe et al., 2000).

392   The combination of siderite, magnetite, hematite and non-crystalline goethite suggests a

393   relatively complex mineralization process that is strongly dependent on biological

394   mechanism. Similar formations of mixed minerals can be achieved by chemical processes,

395   however they often present with other phase combinations including ferrihydrite-goethite-

396   lepidocrocite-magnetite (Hansel et al., 2005) or goethite-hematite-maghemite-magnetite-

397   akaganeite (Ahn et al., 2012). Furthermore, the starting conditions of microbial Fe(III)

398   reduction, such as the use of different starting substrates including hydrous ferric oxide,

399   goethite, hematite, magnetite, carbonates, and Fe(III)-clays, or the variation of geochemical

400   parameters including Eh, pH, and temperature can yield stark differences in the types of

401   minerals produced via primary or secondary mineralization pathways (Jimenez-Lopez et al.,

402   2010; Perez-Gonzalez et al., 2010).

403   Here we suggest that the use of Mössbauer-Raman-XRD analyses in combination with other

404   structural studies could potentially be used to obtain a suitable range of criteria to help

405   develop fingerprints to distinguish biological and abiotic magnetite. The biogenic magnetite

406   and goethite from our experiments differs significantly from the magnetite and goethite

407 observed with the Mars Exploration Rovers in rocks and soils on Mars (Table 1), where the

408 magnetite is suggested to be of primary, igneous origin (Morris et al., 2008).

409 Our biogenic magnetite is non-stoichiometric and, in the case of FH+AQDS-13 appears to

410 be oxidized. The broad lines reflect in Mössbauer spectra reflect low crystallinity, potentially

411 resulting from impurities such as organic matter, and/or small particle sizes. The presence of

412 organic matter is confirmed by Raman spectroscopy and small particle sizes are indicated by

413 XRD. Taken together, the evidence extracted from the different techniques could be used to

414 establish some criteria for bio-signatures. Table 4 presents a resume of the main features of

415 each technique that could be used for the detection of bio-signatures in planetary exploration.

416 The question, however, is whether the features observed here would be preserved over

417 geological timescales. Over time, magnetite might mature and increase in crystallinity while

418 organic matter can undergo decay, thus potentially eliminating any evidence over extended

419 timescales.

420 **Conclusions**

421 The MIMOS II instrument, of which two have previously been sent to Mars onboard Martian

422 rovers, has been used to characterize different mineral phases produced by the microbial

423 reduction of Fe(III)-oxyhydroxide and determined the dominant phase produced to be

424 magnetite. Other techniques on current or future Mars rover missions such as XRD and

425 Raman have been used to complement these results. Mössbauer, XRD, and Raman confirm

426 the existence of magnetite for the samples incubated with only ferrihydrite (FH+AQDS-13

427 and FH-AQDS-13) and magnetite combined with siderite for the sample incubated with an

428 added electron shuttle (FH+AQDS-13). The values of the crystal lattice show values under

429   8.397 Å and crystalline sizes under 30 nm being in the range of superparamagnetism as

430   confirmed by the Mössbauer analysis.

431   Raman analysis shows the formation of different mineralization products, including goethite

432   (possibly), hematite, magnetite and siderite which is only somewhat in agreement with the

433   Mössbauer analyses that did not observe hematite in samples. Some differences between the

434   bio-magnetite and natural magnetite have been detected by Raman spectroscopy on the bands

435   at approximately 650 and 540 cm^{-1}. In all spectra recorded, organic compounds were detected

436   which correspond to the DIRB *G. sulfurreducens*.

437   The combination of these three different analytical techniques could be used as a critical

438   approach for observing the products of Fe-biomineralization processes on future space

439   missions, especially those focused on Mars. In this regard, these techniques, used in

440   combination with morphological studies, will help to establish a criterion of the biological

441   origin of biogenic magnetite and other Fe minerals.

450   **References**

451 Ahn, T., Kim, J.H., Yang, H.M., Lee, J.W., Kim, J.D., 2012. Formation pathways of

452   magnetite nanoparticles by coprecipitation method. J. Phys. Chem. C 116, 6069–6076.

453   doi:10.1021/jp211843g

454 Bish, D.L., Blake, D.F., Vaniman, D.T., Chipera, S.J., Morris, R. V, Ming, D.W., Treiman,

455   A.H., Sarrazin, P., Morrison, S.M., Downs, R.T., Achilles, C.N., Yen, A.S., Bristow,

456   T.F., Crisp, J.A., Morookian, J.M., Farmer, J.D., Rampe, E.B., Stolper, E.M.,

457   Spanovich, N., Team, M.S.L.S., 2013. X-ray Diffraction Results from Mars Science

458   Laboratory: Mineralogy of Rocknest at Gale Crater. Sci. 341.

459   doi:10.1126/science.1238932

460 Blakemore, R., 1975. Magnetotactic bacteria. Sci. 190, 377–379.

461   doi:10.1126/science.170679

462 Bost, N., Ramboz, C., LeBreton, N., Foucher, F., Lopez-Reyes, G., De Angelis, S., Josset,

463   M., Venegas, G., Sanz-Arranz, A., Rull, F., Medina, J., Josset, J.-L., Souchon, A.,

464   Ammannito, E., De Sanctis, M.C., Di Iorio, T., Carli, C., Vago, J.L., Westall, F., 2015.

465   Testing the ability of the ExoMars 2018 payload to document geological context and

466   potential habitability on Mars. Planet. Space Sci. 108, 87–97.

467   doi:10.1016/j.pss.2015.01.006

468 Bost, N., Westall, F., Ramboz, C., Foucher, F., Pullan, D., Meunier, A., Petit, S., Fleischer,

469   I., Klingelhöfer, G., Vago, J.L., 2013. Missions to Mars: Characterisation of Mars

470   analogue rocks for the International Space Analogue Rockstore (ISAR). Planet. Space

471   Sci. 82–83, 113–127. doi:http://dx.doi.org/10.1016/j.pss.2013.04.006

472 Böttger, U., de Vera, J.-P., Fritz, J., Weber, I., Hübers, H.-W., Schulze-Makuch, D., 2012.

473   Optimizing the detection of carotene in cyanobacteria in a martian regolith analogue

474   with a Raman spectrometer for the ExoMars mission. Planet. Space Sci. 60, 356–362.

475   doi:http://dx.doi.org/10.1016/j.pss.2011.10.017

476 Byrne, J.M., Klueglein, N., Pearce, C., Rosso, K.M., Appel, E., Kappler, A., 2015. Redox

477   cycling of Fe(II) and Fe(III) in magnetite by Fe-metabolizing bacteria. Science (80-.).

478   347, 1473–1476. doi:10.1126/science.aaa4834

479 Byrne, J.M., Telling, N.D., Coker, V.S., Pattrick, R.A.D., van der Laan, G., Arenholz, E.,

480   Tuna, F., Lloyd, J.R., 2011. Control of nanoparticle size, reactivity and magnetic

481   properties during the bioproduction of magnetite by Geobacter sulfurreducens.

482   Nanotechnology 22, 455709.

483 Cornell, R.M., Schwertmann, U., 2003. The iron oxydes: structure, Properties, Reactions,

484   Occurences and Uses, in: Wiley-Vch. p. ISBN: 3-527-30274-3.

485   doi:10.1002/3527602097

486 Da Costa, G.M., De Grave, E., De Bakker, P.M.A., Vandenberghe, R.E., 1995. Influence of

487   nonstoichiometry and the presence of maghemite on the Mössbauer spectrum of

488   magnetite. Clays Clay Miner. 43, 656–668.

489 Daniels, J.M., Rosencwaig, A., 1969. Mössbauer spectroscopy of stoichiometric and non-

490   stoichiometric magnetite. J. Phys. Chem. Solids 30, 1561–1571. doi:10.1016/0022-

491   3697(69)90217-0

492 de Faria, D.L.A., Silva, S.V., de Oliveira, M.T., 1997. Raman microspectroscopy of some

493   iron oxides and oxyhydroxides. J. Raman Spectrosc. 28, 873–878.

494 Dezsi, I., Fetzer, C., Gombköt, Á., Szucs, I., Gubicza, J., Ungár, T., 2008. Phase transition

495   in nanomagnetite. J. Appl. Phys. 103, 1–5. doi:10.1063/1.2937252

496   Dippon, U., Schmidt, C., Behrens, S., Kappler, A., Dippon, U.R.S., Schmidt, C., Behrens,

497   S., Kappler, A., 2015. Secondary Mineral Formation During Ferrihydrite Reduction by

498   Shewanella oneidensis MR-1 Depends on Incubation Vessel Orientation and Resulting

499   Gradients of Cells , Fe and Fe Minerals. Geomicrobiol. J. 451.

500   doi:10.1080/01490451.2015.1017623

501   Ehrenreich, A., Widdel, F., 1994. Anaerobic oxidation of ferrous iron by purple bacteria, a

502   new type of phototrophic metabolism. Appl. Environ. Microbiol. 60, 4517–4526.

503   el-Kabbani, O., Chang, C.H., Tiede, D., Norris, J., Schiffer, M., 1991. Comparison of

504   reaction centers from Rhodobacter sphaeroides and Rhodopseudomonas viridis:

505   overall architecture and protein-pigment interactions. Biochemistry 30, 5361–5369.

506   Ferrari, A.C., 2007. Raman spectroscopy of graphene and graphite: Disorder, electron-

507   phonon coupling, doping and nonadiabatic effects. Solid State Commun. 143, 47–57.

508   Grossman, L., 2013. NASA urged to seek live Martians with 2020 rover. New Sci. 219, 9.

509   doi:10.1016/S0262-4079(13)61775-3

510   Hanesch, M., 2009. Raman spectroscopy of iron oxides and (oxy)hydroxides at low laser

511   power and possible applications in environmental magnetic studies. Geophys. J. Int.

512   177, 941–948. doi:10.1111/j.1365-246X.2009.04122.x

513   Hansel, C.M., Benner, S.G., Fendorf, S., 2005. Competing Fe (II)-induced mineralization

514   pathways of ferrihydrite. Environ. Sci. Technol. 39, 7147–7153.

515   doi:10.1021/es050666z

516   Hansel, C.M., Benner, S.G., Neiss, J., Dohnalkova, A., Kukkadapu, R.K., Fendorf, S.,

517   2003. Secondary mineralization pathways induced by dissimilatory iron reduction of

518   ferrihydrite under advective flow. Geochim. Cosmochim. Acta 67, 2977–2992.

519   Helgason, O., 2004. Processes in geophysics studied by Mossbauer spectroscopy.

520   Hyperfine Interact. 156, 379–388. doi:10.1023/B:HYPE.0000043257.28606.14

521   Hermosilla, I., Lopez-Reyes, G., Catala, A., Sanz, A., Llanos, D.R., Rull, F., 2012. Raman

522   spectra processing algorithms and database for RLS-ExoMars. Proc. Eur. Planet. Sci.

523   Congr. 7, 23–28.

524   Hutchinson, I.B., Parnell, J., Edwards, H.G.M., Jehlicka, J., Marshall, C.P., Harris, L. V,

525   Ingley, R., 2014. Potential for analysis of carbonaceous matter on Mars using Raman

526   spectroscopy. Planet. Space Sci. doi:http://dx.doi.org/10.1016/j.pss.2014.07.006

527   ICDD, n.d. PDF-2 database.

528   James, F., 2004. MINUIT Tutorial, Function Minimization, in: CERN Computing and Data

529   Processing School. Pertisau, pp. 10–24.

530   Jimenez-Lopez, C., Romanek, C.S., Bazylinski, D.A., 2010. Magnetite as a prokaryotic

531   biomarker: A review. J. Geophys. Res. 115, G00G03. doi:10.1029/2009JG001152

532   Kappler, A., Newman, D.K., 2004. Formation of Fe(III)-minerals by Fe(II)-oxidizing

533   photoautotrophic bacteria. Geochim. Cosmochim. Acta 68, 1217–1226.

534   doi:10.1016/j.gca.2003.09.006

535   Kappler, A., Schink, B., Newman, D.K., 2005. Fe(III) mineral formation and cell

536   encrustation by the nitrate-dependent Fe(II)-oxidizer strain BoFeN1. Geobiology 3,

537   235–245. doi:10.1111/j.1472-4669.2006.00056.x

538   Kappler, A., Straub, K.L., 2005. Geomicrobiological Cycling of Iron. Rev. Mineral.

539   Geochemistry 59, 85–108. doi:10.2138/rmg.2005.59.5

540   Klingelhöfer, G., Morris, R. V, Bernhardt, B., Rodionov, D., de Souza, P.A., Squyres,

541   S.W., Foh, J., Kankeleit, E., Bonnes, U., Gellert, R., Schröder, C., Linkin, S., Evlanov,

542   E., Zubkov, B., Prilutski, O., 2003. Athena MIMOS II Mössbauer spectrometer

543   investigation. J. Geophys. Res. Planets 108, n/a--n/a. doi:10.1029/2003JE002138

544   Klingelhöfer, G., Morris, R. V, Bernhardt, B., Schröder, C., Rodionov, D.S., de Souza,

545   P.A., Yen, A., Gellert, R., Evlanov, E.N., Zubkov, B., Foh, J., Bonnes, U., Kankeleit,

546   E., Gütlich, P., Ming, D.W., Renz, F., Wdowiak, T., Squyres, S.W., Arvidson, R.E.,

547   2004. Jarosite and Hematite at Meridiani Planum from Opportunity's Mössbauer

548   Spectrometer. Sci. 306, 1740–1745. doi:10.1126/science.1104653

549   Kudelski, A., 2005. Characterization of thiolate-based mono- and bilayers by vibrational

550   spectroscopy: A review. Vib. Spectrosc.

551   Lalla, E.A., López-Reyes, G., Sansano, A., Sanz-Arranz, A., Schmanke, D., Klingelhöfer,

552   G., Medina-García, J., Martínez-Frías, J., Rull-Pérez, F., 2015. Estudio

553   espectroscópico y DRX de afloramientos terrestres volcánicos en la isla de Tenerife

554   como posibles análogos de la geología marciana. Estud. Geológicos 71, 1–19.

555   doi:10.3989/egeol.41927.354

556   Lalla, E.A., Sanz-Arranz, A., Lopez-Reyes, G., Sansano, A., Medina, J., Schmanke, D.,

557   Klingelhoefer, G., Rodríguez-Losada, J.A., Martínez-Frías, J., Rull, F., 2016. Raman–

558   Mössbauer–XRD studies of selected samples from "Los Azulejos" outcrop: A possible

559   analogue for assessing the alteration processes on Mars. Adv. Sp. Res. 57, 2385–2395.

560   doi:10.1016/j.asr.2016.03.014

561   Léveillé, R., 2009. Validation of astrobiology technologies and instrument operations in

562   terrestrial analogue environments. Comptes Rendus Palevol 8, 637–648.

563   doi:http://dx.doi.org/10.1016/j.crpv.2009.03.005

564   Liu, H., Li, P., Lu, B., Wei, Y., Sun, Y., 2009. Transformation of ferrihydrite in the

565   presence or absence of trace Fe(II): The effect of preparation procedures of

566   ferrihydrite. J. Solid State Chem. 182, 1767–1771.

567   Lovley, D.R., Phillips, E.J.P., 1988. Novel Mode of Microbial Energy Metabolism: Organic

568   Carbon Oxidation Coupled to Dissimilatory Reduction of Iron or Manganese. Appl.

569   Envir. Microbiol. 54, 1472–1480.

570   Lovley, D.R., Phillips, E.J.P., 1986. Availability of Ferric Iron for Microbial Reduction in

571   Bottom Sediments of the Freshwater Tidal Potomac River. Appl. Envir. Microbiol. 52,

572   751–757.

573   Magnetite - www.mindat.org [WWW Document], 2001. URL http://www.mindat.org/min-

574   2538.html

575   Moon, J.-W., Rawn, C.J., Rondinone, A.J., Wang, W., Vali, H., Yeary, L.W., Love, L.J.,

576   Kirkham, M.J., Gu, B., Phelps, T.J., 2010. Crystallite Sizes and Lattice Parameters of

577   Nano-Biomagnetite Particles. J. Nanosci. Nanotechnol. 10, 8298–8306.

578   Morris, R. V., Klingelhöfer, G., Schröer, C., Fleischer, I., Ming, D.W., Yen, A.S., Gellert,

579   R., Arvidson, R.E., Rodionov, D.S., Crumpler, L.S., Clark, B.C., Cohen, B.A.,

580   McCoy, T.J., Mittlefehldt, D.W., Schmidt, M.E., De Souza, J.A., Squyres, S.W., 2008.

581   Iron mineralogy and aqueous alteration from Husband Hill through Home Plate at

582   Gusev Crater, Mars: Results from the Mössbauer instrument on the Spirit Mars

583   Exploration Rover. J. Geophys. Res. E Planets 113.

584   Morris, R. V, Klingelhöfer, G., Bernhardt, B., Schröder, C., Rodionov, D.S., de Souza,

585   P.A., Yen, A., Gellert, R., Evlanov, E.N., Foh, J., Kankeleit, E., Gütlich, P., Ming,

586   D.W., Renz, F., Wdowiak, T., Squyres, S.W., Arvidson, R.E., 2004. Mineralogy at

587   Gusev Crater from the Mössbauer Spectrometer on the Spirit Rover. Science (80-.).

588   305, 833 LP-836.

589   Morris, R. V, Klingelhöfer, G., Schröder, C., Rodionov, D.S., Yen, A., Ming, D.W., de

590   Souza, P.A., Fleischer, I., Wdowiak, T., Gellert, R., Bernhardt, B., Evlanov, E.N.,

591   Zubkov, B., Foh, J., Bonnes, U., Kankeleit, E., Gütlich, P., Renz, F., Squyres, S.W.,

592   Arvidson, R.E., 2006. Mössbauer mineralogy of rock, soil, and dust at Gusev crater,

593   Mars: Spirit's journey through weakly altered olivine basalt on the plains and

594   pervasively altered basalt in the Columbia Hills. J. Geophys. Res. Planets 111, n/a--

595   n/a. doi:10.1029/2005JE002584

596   Morris, R. V, Ruff, S.W., Gellert, R., Ming, D.W., Arvidson, R.E., Clark, B.C., Golden,

597   D.C., Siebach, K., Klingelhöfer, G., Schröder, C., Fleischer, I., Yen, A.S., Squyres,

598   S.W., 2010. Identification of Carbonate-Rich Outcrops on Mars by the Spirit Rover.

599   Sci. 329, 421–424. doi:10.1126/science.1189667

600   Nixon, S.L., Cockell, C.S., Tranter, M., 2012. Limitations to a microbial iron cycle on

601   Mars. Planet. Space Sci. 72, 116–128. doi:10.1016/j.pss.2012.04.003

602   O'Loughlin, E.J., Gorski, C.A., Scherer, M.M., Boyanov, M.I., Kemner, K.M., 2010.

603   Effects of Oxyanions, Natural Organic Matter, and Bacterial Cell Numbers on the

Bioreduction of Lepidocrocite (γ-FeOOH) and the Formation of Secondary

Mineralization Products. Environ. Sci. Technol. 44, 4570–4576.

doi:10.1021/es100294w

Parenteau, M.N., Jahnke, L.L., Farmer, J.D., Cady, S.L., 2014. Production and Early

Preservation of Lipid Biomarkers in Iron Hot Springs. Astrobiology 14, 502–521.

doi:10.1089/ast.2013.1122

Pereira, B.G., Vianna-Soares, C.D., Righi, A., Pinheiro, M.V.B., Flores, M.Z.S., Bezerra,

E.M., Freire, V.N., Lemos, V., Caetano, E.W.S., Cavada, B.S., 2007. Identification of

lamivudine conformers by Raman scattering measurements and quantum chemical

calculations. J. Pharm. Biomed. Anal. 43, 1885–1889.

Perez-Gonzalez, T., Jimenez-Lopez, C., Neal, A.L., Rull-Perez, F., Rodriguez-Navarro, A.,

Fernandez-Vivas, A., Iañez-Pareja, E., 2010. Magnetite biomineralization induced by

Shewanella oneidensis. Geochim. Cosmochim. Acta 74, 967–979.

doi:10.1016/j.gca.2009.10.035

Piepenbrock, A., Dippon, U., Porsch, K., Appel, E., Kappler, A., 2011. Dependence of

microbial magnetite formation on humic substance and ferrihydrite concentrations.

Geochim. Cosmochim. Acta 75, 6844–6858. doi:10.1016/j.gca.2011.09.007

Rietveld, H.M., 1969. A profile refinement method for nuclear and magnetic structures. J.

Appl. Crystallogr. 2, 65–71. doi:10.1107/S0021889869006558

Rodríguez-Carvajal, J., 1993. Recent advances in magnetic structure determination by

neutron powder diffraction. Phys. B Condens. Matter 192, 55–69.

doi:http://dx.doi.org/10.1016/0921-4526(93)90108-I

626   Rothschild, L.J., Mancinelli, R.L., 2001. Life in extreme environments. Nature 409, 1092–

627   1101.

628   Ruecker, A., Schröder, C., Byrne, J., Weigold, P., Behrens, S., Kappler, A., 2016.

629   Geochemistry and Mineralogy of Western Australian Salt Lake Sediments:

630   Implications for Meridiani Planum on Mars. Astrobiology 16, 525–538.

631   doi:10.1089/ast.2015.1429

632   Rull, F., Martinez-Frias, J., Rodríguez-Losada, J.A., 2007. Micro-Raman spectroscopic

633   study of El Gasco pumice, western Spain. J. Raman Spectrosc. 38, 239–244.

634   doi:10.1002/jrs.1628

635   Rull, F., Martinez-Frias, J., Sansano, A., Medina, J., Edwards, H.G.M., 2004. Comparative

636   micro-Raman study of the Nakhla and Vaca Muerta meteorites. J. Raman Spectrosc.

637   35, 497–503. doi:10.1002/jrs.1177

638   Sansano-Caramazana, A., 2015. Síntesis y caracterización espectroscópica de sulfatos de

639   hierro: implicaciones en astrobiología y la exploración de Marte. University of

640   Valladolid.

641   Sansano, A., Navarro, R.J., Manrique, J.A., Medina, J., Rull, F., 2015. Multispectral

642   Analysis of Mars Analog Altered Volcanic Materials from Faroe Islands. Implicatons

643   for Missions as ExoMars and Mars 2020. Lunar Planet. Sci. Conf.

644   Scherrer, P., 1918. Bestimmung der Grösse und der inneren Struktur von Kolloidteilchen

645   mittels Röntgenstrahlen. Nachrichten von der Gesellschaft der Wissenschaften zu

646   Göttingen, Math. Klasse 1918, 98–100. doi:10.1007/978-3-662-33915-2

647   Schröder, C., 2003. ATHENA Reference Samples. Mainz.

648   Shebanova, O.N., Lazor, P., 2003. Raman spectroscopic study of magnetite (FeFe2O4): a

649   new assignment for the vibrational spectrum. J. Solid State Chem. 174, 424–430.

650   doi:10.1016/S0022-4596(03)00294-9

651   Stookey, L.L., 1970. Ferrozine---a new spectrophotometric reagent for iron. Anal. Chem.

652   42, 779–781.

653   Vandenberghe, R.E., Barrero, C.A., da Costa, G.M., Van San, E., De Grave, E., 2000.

654   Mössbauer characterization of iron oxides and (oxy)hydroxides: the present state of

655   the art. Hyperfine Interact. 126, 247–259. doi:10.1023/A:1012603603203

656   Veeramani, H., Alessi, D.S., Suvorova, E.I., Lezama-Pacheco, J.S., Stubbs, J.E., Sharp,

657   J.O., Dippon, U., Kappler, A., Bargar, J.R., Bernier-Latmani, R., 2011. Products of

658   abiotic U(VI) reduction by biogenic magnetite and vivianite. Geochim. Cosmochim.

659   Acta 75, 2512–2528. doi:10.1016/j.gca.2011.02.024

660   Wang, A., Korotev, R.L., Jolliff, B.L., Ling, Z., 2015. Raman imaging of extraterrestrial

661   materials. Planet. Space Sci. 112, 23–34. doi:10.1016/j.pss.2014.10.005

662   Wohlfarth, E.P., Arrott, A.S., 1982. Ferromagnetic Materials: A Handbook on the

663   Properties of Magnetically Ordered Substances, Vols. 1 and 2, Physics Today.

664   doi:10.1063/1.2914974

665   Zegeye, A., Abdelmoula, M., Usman, M., Hanna, K., Ruby, C., 2011. In situ monitoring of

666   lepidocrocite bioreduction and magnetite formation by reflection Mössbauer

667   spectroscopy. Am. Mineral. 96, 1410–1413. doi:10.2138/am.2011.3794

668   Zegeye, a, Mustin, C., Jorand, F., 2010. Bacterial and iron oxide aggregates mediate

669   secondary iron mineral formation: green rust versus magnetite. Geobiology 8, 209–22.

670

671

List of Figure

Figure 1 - MIMOS II analysis from the 2014 experiments (a) in situ measurement 6 hours after start FH-AQDS on the MIMOS II, (b) in situ measurement 19 days after start FH-AQDS on the MIMOS II, (c) filtered sample room temperature FH-AQDS.

Figure 2 - MIMOS II analysis from the 2013 experiments (a) FH-AQDS measured at room temperature; (b) FH+AQDS measured at room temperature; (c) Magnetite (Athena Reference Sample 043).

Figure 3 - XRD pattern for FH-AQDS and FH+AQDS. Samples show a broad reflection between 5° and 15° 2θ due to the Kapton film (Kp) in which they were sealed.

Figure 4. (A) Raman Spectra from 100 to 2000 cm^{-1} of (a) and (b) Magnetite prepared in the absence of AQDS (FH-AQDS); (c) and (d) Magnetite prepared in the presence of AQDS (FH+AQDS). Assignment of the most intense Raman vibration: Hematite, Magnetite, Goethite, Siderite, GS (G. sulfurreducens) and C-C (Carbon vibration). (B) Raman spectra from 2000 to 3000 cm^{-1} of (a) and (b) Magnetite prepared in the absence of AQDS (FH-AQDS); (c) and (d) Magnetite prepared in the presence of AQDS (FH+AQDS). Assignment of the most intense Raman vibration: C-H (C-H (Organics) and GS (G. sulfurreducens). (C) Gaussian band fitting of the regions: 200-420 cm^{-1} and 600 to 800 cm^{-1}.
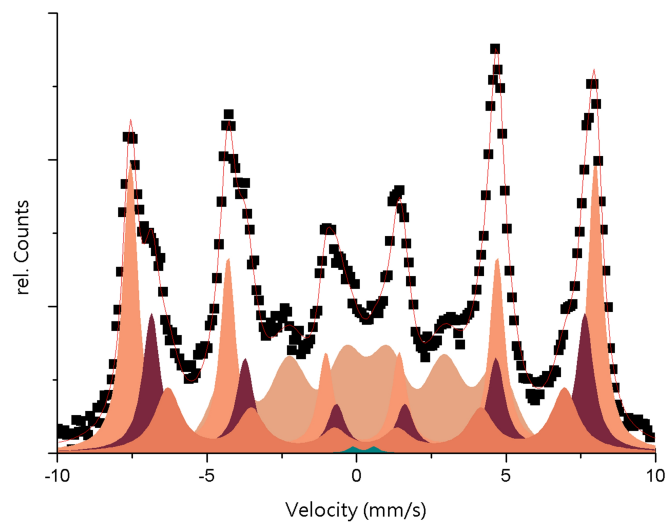
a)

b)

c)
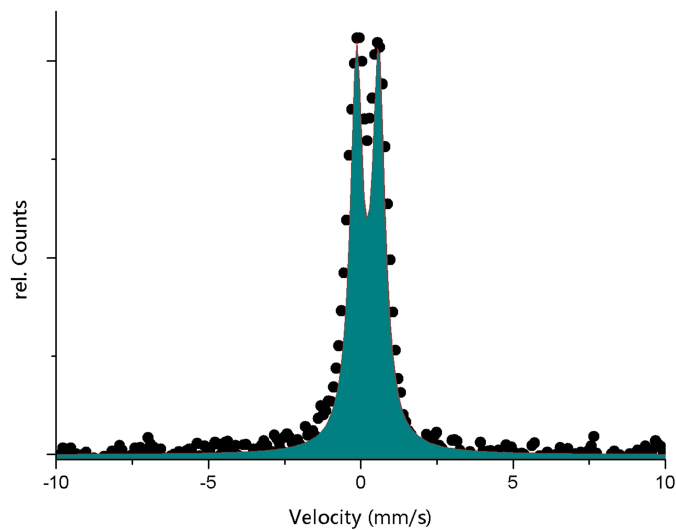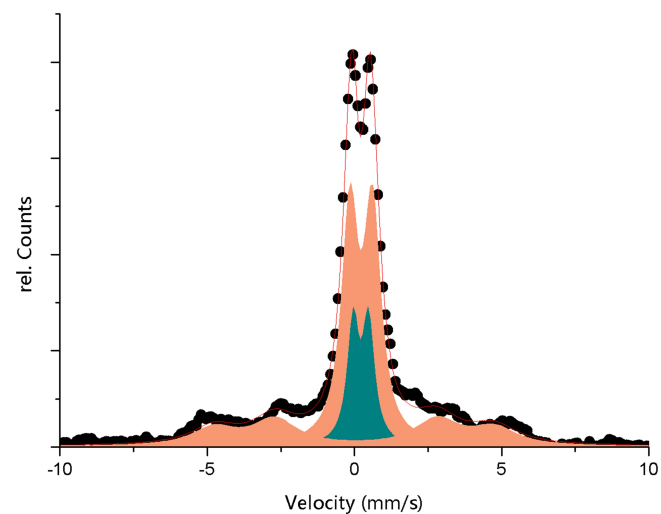
- Data
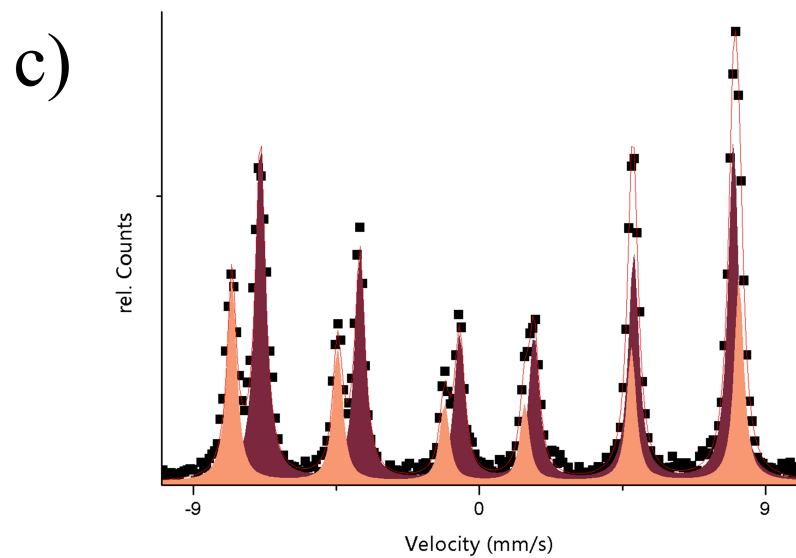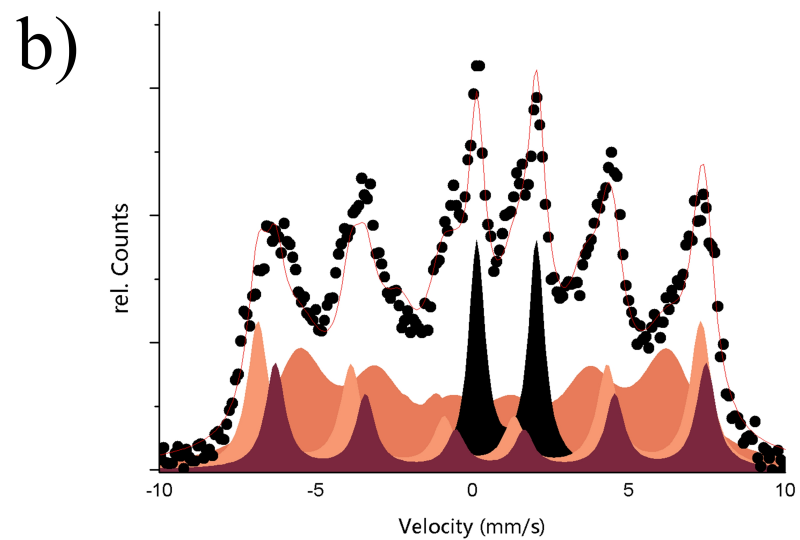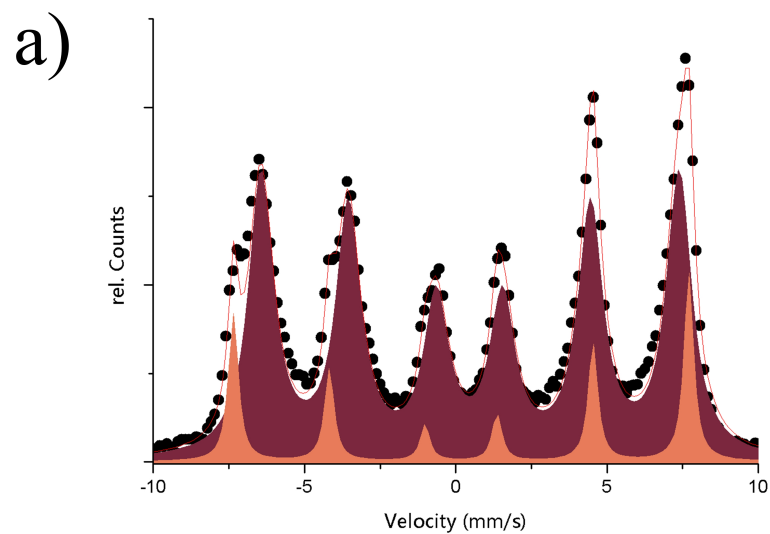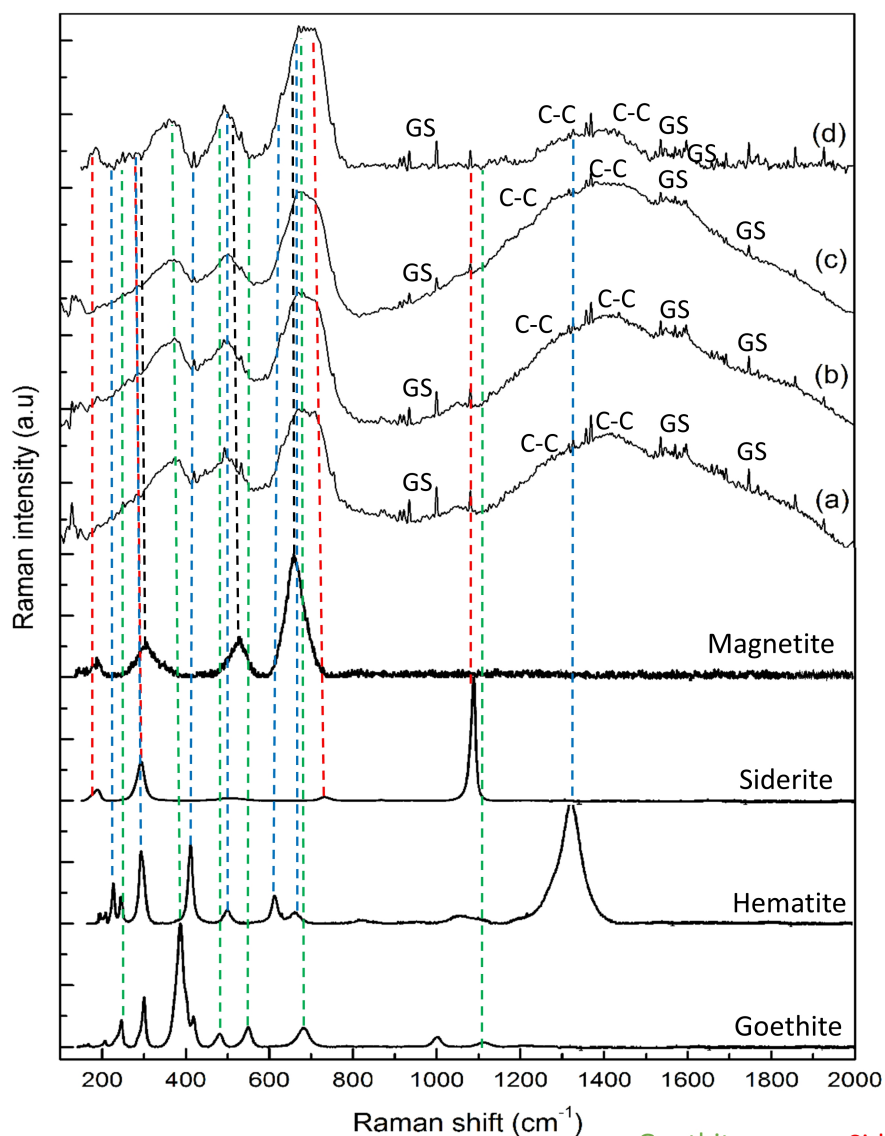- Magnetite (tet^{3+})
- Magnetite (oct$^{2.5+}$)
- Goethite nanophase
- Magnetite nanophase
- Ferrihydrite
- Siderite
- Fit

a)

b)

c)

Data
Magnetite (tet^{3+})
Magnetite (oct$^{2.5+}$)
Magnetite nanophase
Siderite
Fit

(A)

(d)

(c)

(b)

(a)

GS — *G. sulfurreducens*; C-C — Carbon vibration; GS markers

Magnetite

Siderite

Hematite

Goethite

Raman intensity (a.u)
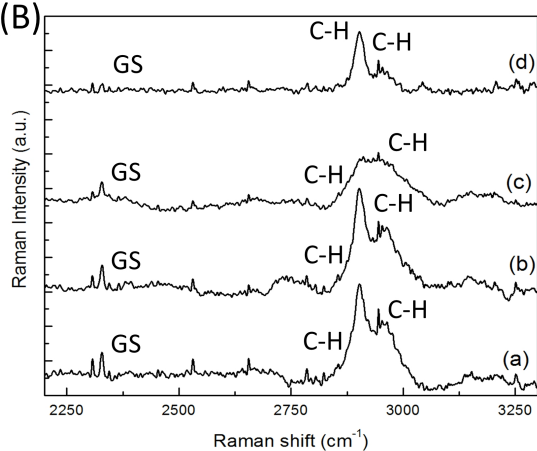
Raman shift (cm^{-1})

(a) and (b) Magnetite prepared in the absence of AQDS (FH-AQDS)
(c) and (d) Magnetite prepared in the presence of AQDS (FH+AQDS)

Goethite   Siderite
Hematite   Magnetite

(B)

GS   C-H   C-H   (d)

GS   C-H   C-H   (c)

GS   C-H   C-H   (b)

GS   C-H   C-H   (a)

Raman Intensity (a.u.)

Raman shift (cm^{-1})

GS (*G. sulfurreducens*), C-C (Carbon vibration) and
C-H (C-H (Organics))

(C)

303 335 360 381   650   692   (d)
283   662 683

281 325 362 384   636 660 698   (c)
           384   620

250 284 318 345 360 380 616 630 660 696   (b)
                              683

250 283 320 345 358 380 620 663 700   (a)
                              683

Raman Intensity (a.u.)

Raman shift (cm^{-1})
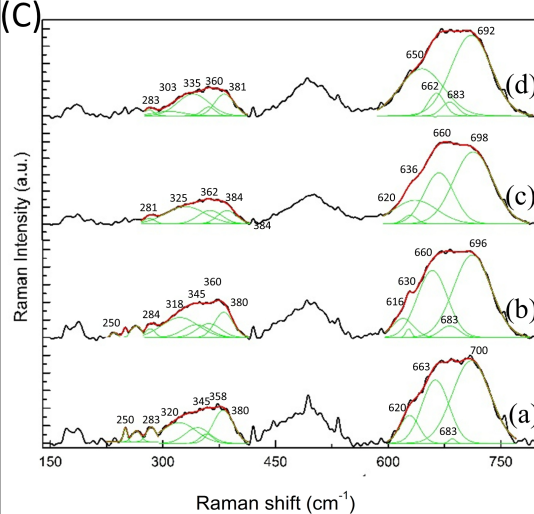
List of Tables:

Table 1. Mössbauer parameters of experimental and Martian samples.

Table 2. Bands used as diagnostic for the curve fitting identification of principal iron oxide phases.

Table 3. (a) Raman general position in curve fitting of the Raman spectra from FH+AQDS-13 and FH-AQDS-13 samples. (b) Raman Curve analysis per spectra corresponding to Figure 3 and its possible mineral assignments compared to standards.

Table 4. Comparison of the main features of Mössbauer, XRD, and Raman that can be used for potential bio-mineral detection.

Table 1

Sample	Mineral Phase	CS (δ) mm s^{-1}	Linewidth (S) mm s^{-1}	ΔE_Q mm s^{-1}	B_{hf} T	Relative area %	Fe(II)/Fe(III) in Fe$_3$O$_4$
FH-AQDS-14 (*in situ*, 6 h)	Ferrihydrite	0.34	0.25	0.74		100	
FH-AQDS-14 (*in situ*, 19 days)	Ferrihydrite	0.34	0.34	0.77		11.4	
	Magnetite nanophase[a]	0.33	0.24	0.53		21.7	
	Magnetite nanophase[b]	0.13	0.92	-0.03	29.5	66.9	
FH-AQDS-14 (filtered)	Ferrihydrite	0.34	0.20	0.74		0.5	
	Magnetite (tet- Fe^{3+})	0.30	0.30	0.00	48.1	40.1	
	Magnetite (oct- Fe$^{2,5+}$)	0.54	0.34	- 0.04	44.9	21.7	
	Magnetite nanophase[b]	0.43	0.54	0.00	41.2	15.8	
	Goethite nanophase	0.39	0.35	-0.06	27.6	21.9	
FH-AQDS-13 (filtered)	Magnetite (tet-Fe^{3+})	0.30	0.19	0.00	46.6	20.8	
	Magnetite (oct- Fe$^{2,5+}$)	0.56	0.52	-0.00	42.8	79.2	0.65
FH+AQDS-13	Magnetite (tet-Fe^{3+})	0.33	0.40	0.00	44.0	18.6	
	Magnetite (oct- Fe$^{2,5+}$)	0.69	0.36	0.01	42.8	12.1	0.25
	Magnetite nanophase[b]	0.45	1.07	0.01	36.6	35.7	
	Magnetite nanophase[b]	0.71	0.59	0.04	18.0	11.4	
	Siderite	1.21	0.31	1.90		22.2	
Athena Reference Sample 043	Magnetite (tet-Fe^{3+})	0.29	0.2	0.01	49.4	37.1	
	Magnetite (oct- Fe$^{2,5+}$)	0.66	0.2	0.00	46.1	62.9	0.46
Average Mars magnetite[c]	Magnetite (tet-Fe^{3+})	0.31±0.03		0.01±0.03	50.0±0.5		
	Magnetite (oct- Fe$^{2,5+}$)	0.66±0.06		-0.01±0.08	46.7±0.8		
Average Mars goethite[c]	Goethite	0.38±0.02		-0.19±0.10	37.3±2.9		

[a]Superparamagnetic magnetite - magnetic ordering prevented by small particle size.

[b]Magnetically ordered magnetite that has not reached full hyperfine splitting because of small particle size and/or impurities

[c]Values from Morris et al. (2008), averaging all magnetite and goethite measurements obtained in Gusev Crater with Mars Exploration Rover Spirit. Uncertainties quoted are standard deviations (2σ).

Table 2.

Mineral Phase	Principal Raman bands (cm^{-1})
Goethite	244, 299, **385**, 480, 681
Hematite	**225,** 245, 290-300, 412
Lepidocrocite	**250**, 348, 379, 528, 650
Siderite	184, 287, 722, **1082**
Ferrihydrite	370, 510, **710**
Magnetite	310, 540, **670**
Maghemite	350, 512, **665**, **730**

Table 3 a.

Raman band position (cm^{-1})	Raman assignment
172 (w)	*****
186 (w)	Siderite
283 (m)	Hematite/Goethite/Siderite
340 (m)	Magnetite
378 (m)	Hematite/Goethite
420 (vw)	Goethite
451 (sh)	****
474 (m)	Goethite
495 (s)	Siderite/Magnetite
533 (sh)	Magnetite
650 (sh)	****
667 (vs)	Magnetite
717 (vs)	Siderite
755 (sh)	*G. sulfurreducens*
1000 (w)	*G. sulfurreducens*
1082 (w)	Siderite
1314 (m)	Hematite/Goethite
1358 (w)	*G. sulfurreducens*
1370 (w)	*G. sulfurreducens*
1422 (m)	Carbon vibration
1565 (m)	Carbon vibration
1598 (w)	*G. sulfurreducens*
2328 (w)	*G. sulfurreducens*
2903 (s)	C-H(Organics)
2961 (m)	C-H (Organics)

**** Raman band not assigned

Table 3 b.

Mineral Phase	Principal Raman fitting bands (cm^{-1}) of the Mineral and organics detected			
	Raman Spectra (a)	Raman spectra (b)	Raman spectra (c)	Raman Spectra (d)
Goethite	283, **376**, 420, 475	284, **373**, 471	285, **383**, 420	283, **385**, 420, 480
Hematite	**250**, 283, 493, 609, 1348	**250**, 283, 401, 497, 609, 1337	**250**, 283, 403, 480, 1358	**250**, 283, 491, 609, 1331
Siderite	**187**, 505, 711, **1083**	**188**, 504, 703, **1083**	**187**, 700, **1083**	**184**, 712, **1083**
Magnetite	308, 533, **653** or **691** *(bio-mag)**	315, 534, **652** or **679** *(bio-mag)**	308, 534, **642** or **685** *(bio-mag)**	315, 533, **652** or **690** *(bio-mag)**
Organics	1327, **1370**, 1400, 1537,**1598**, 2328, 2344, 2884, **2902**, **2963**	1279, **1386**, 1431, 1549, **1598**, 2307, 2328, 2874, 2902, **2963**	**1287**, 1427, 1559, **1600**, 2328, 2878, **2905**, 2940, 2974	1270, **1401**,1438, 1469, 1542, **1597**, 2874, **2903**, 2947, **2969**, 3043

*Refers to the magnetite produced by *G. sulfurreducens*. The curve fitting relative band intensity of I_{685-90}/I_{650} shows for: (a) ~1.50, (b) 1.27, (c) 1.63, (d) 1.2.

Table 4.

Technique	Structure and crystallinity	Particle size	Detection of organics	Oxidation states	Stoichiometry	*Geological context
Raman spectroscopy	Yes	No	Yes	No	Potentially	Yes
XRD	Yes	Yes	No	No	No	Potentially
Mössbauer Spectroscopy[a]	Yes	Yes	No	Fe	Yes	Yes

[a]Mössbauer spectroscopy is limited to Fe-bearing materials.

***Geological Context: Mineral assemblages and accompanying minerals**